Supporting Information

Interplay of Structural and Compositional Effects on Carrier Recombination in Mixed-Halide Perovskites

Eric M. Talbert[1], Holly F. Zarick[1], Noah J. Orfield[2], Wei Li[3], William R. Erwin[1], Zachary R. DeBra[1], Kemar R. Reid[4], Christopher P. McDonald[5], James R. McBride[2], Jason Valentine[3], Sandra J. Rosenthal[1,2], and Rizia Bardhan[1]

[1]Department of Chemical and Biomolecular Engineering, [2]Department of Chemistry, [3]Department of Mechanical Engineering, [4]Interdisciplinary Graduate Program in Materials Science, Vanderbilt University, Nashville, Tennessee, 37235, USA, [5]Department of Physics and Astronomy, Austin Peay State University, Clarksville, Tennessee, 37044, USA

Table S1. Average grain diameters from AFM image analysis and crystallite diameters from the Scherrer equation. Error from image analysis is the standard deviation.

Spin solvent	Method	x = 0	x = 0.1	x = 0.2	x = 0.33
DMF	Image	55 ± 10 nm	55 ± 10 nm	50 ± 8 nm	50 ± 10 nm
	Scherrer	26.4 nm	13.3 nm	18.5 nm	19.5 nm
DMSO:GBL	Image	200 ± 40 nm	200 ± 35 nm	210 ± 40 nm	180 ± 50 nm
	Scherrer	52.3 nm	41.7 nm	40.8 nm	43.0 nm

Table S2. Stoichiometries obtained from in-situ EDX spectra of $MAPb(I_{1-x}Br_x)_3$ from DMF to indicate that beam induced degradation in the SEM occurs on the scale of minutes. Since all SEM images were taken in the first few seconds of exposure, the bright spots seen in SEM are $MAPbI_3$-rich nuclei rather than resulting from beam damage of samples.

Precursor Br content	Time (min)	X:Pb ratio	EDX Br content
x = 0	0	2.82	0
	1	2.75	0
	5	2.62	0
x = 0.1	0	2.84	0.094
	1	2.80	0.092
	5	2.56	0.089
x = 0.2	0	2.78	0.198
	1	2.74	0.191
	5	2.58	0.189
x = 0.33	0	2.78	0.331
	1	2.71	0.326
	5	2.59	0.323

We obtained in-situ EDX spectra, using 15 keV accelerating voltage and 1.8 nA probe current to achieve sufficient X-ray collection. The nearly 3:1 ratio of halide to lead in EDX spectral fits after a 10 second integration time indicates that the surface is predominantly perovskite (rather than PbI2). While degradation appears on the scale of minutes (Table S2), all SEM images were taken in the first few seconds of exposure, a time scale wherein the lower voltage and current of the beam is expected to produce minimal sample damage.

Table S3. Complete lifetime data from biexponential fits of tr-PL decays of $MAPb(I_{1-x}Br_x)_3$ films.

Spin solvent	Parameter	Bromine Content			
		x = 0	x = 0.1	x = 0.2	x = 0.33
DMF	τ_1	11.53 ns	14.70 ns	11.06 ns	16.03 ns
	τ_2	67.16 ns	116.1 ns	91.66 ns	98.52 ns
	A_1	0.6962	0.8045	0.6414	0.5637
	A_2	0.3362	0.2112	0.4072	0.4878
	τ_{avg}	**29 ns**	**35 ns**	**41 ns**	**52 ns**
DMSO:GBL	τ_1	0.7813 ns	1.127 ns	6.036 ns	4.834 ns
	τ_2	2.682 ns	5.328 ns	n/A	18.81 ns
	A_1	0.4657	0.5935	1.0	0.7281
	A_2	0.6085	0.4103	n/A	0.3043
	τ_{avg}	**1.9 ns**	**2.8 ns**	**6.0 ns**	**8.9 ns**

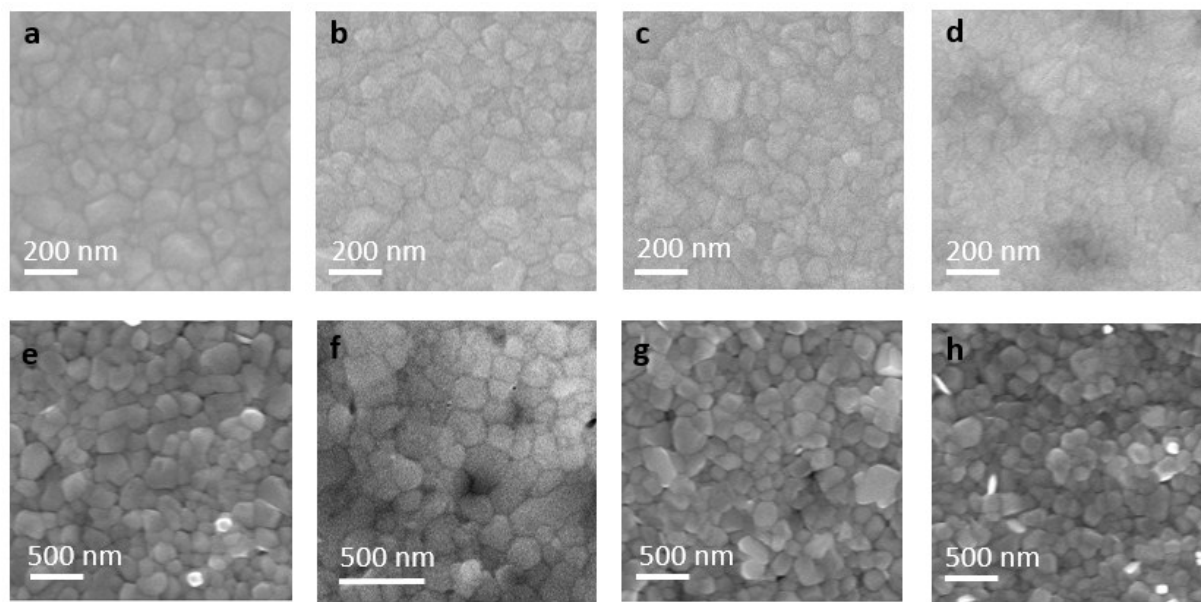**Figure S1.** SEM micrographs of MAPb($I_{1-x}Br_x)_3$ show that grain morphology is consistent across Br compositions. Images (a)-(d) are top-views of perovskite films deposited from DMF with x=0, 0.1, 0.2, and 0.33, and (e)-(h) are films deposited from DMSO:GBL with x=0, 0.1, 0.2, and 0.33, respectively.
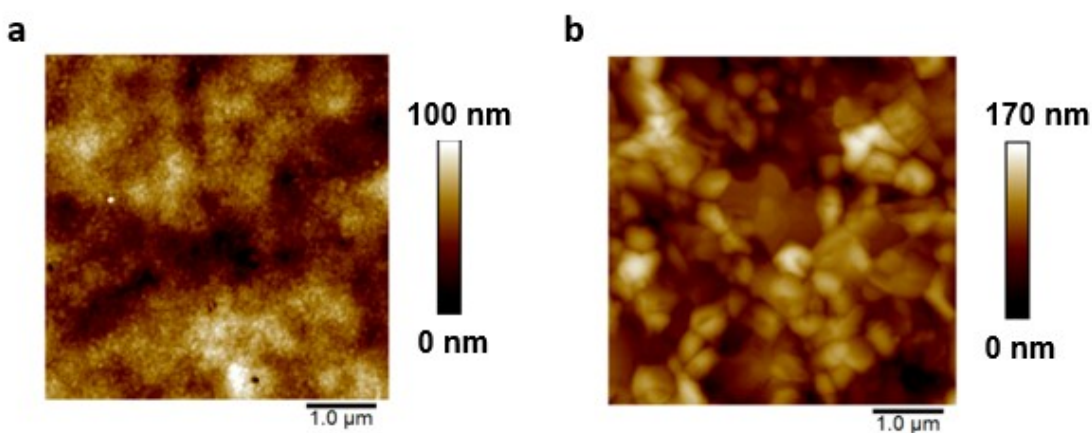

Figure S2. Atomic force micrographs of MAPb($I_{1-x}Br_x)_3$, x=0.20 perovskite films spin-coated from (a) DMF and (b) 3:7 DMSO:GBL. Grain size analysis was performed using Gwiddion 8.0 to segregate grains by brightness and contrast. Averages for each Br composition (x=0, 0.1, 0.2, and 0.33) were calculated from grain size identification on a single representative micrograph of the sample.
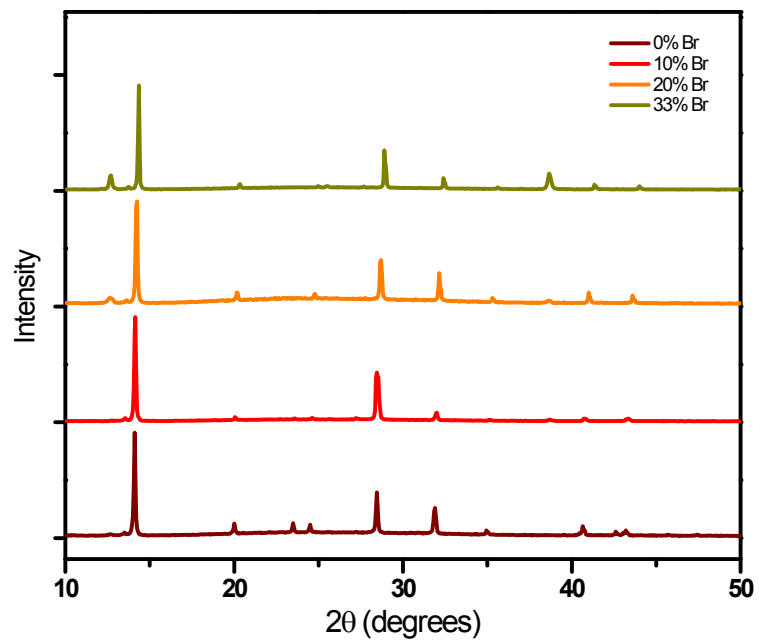
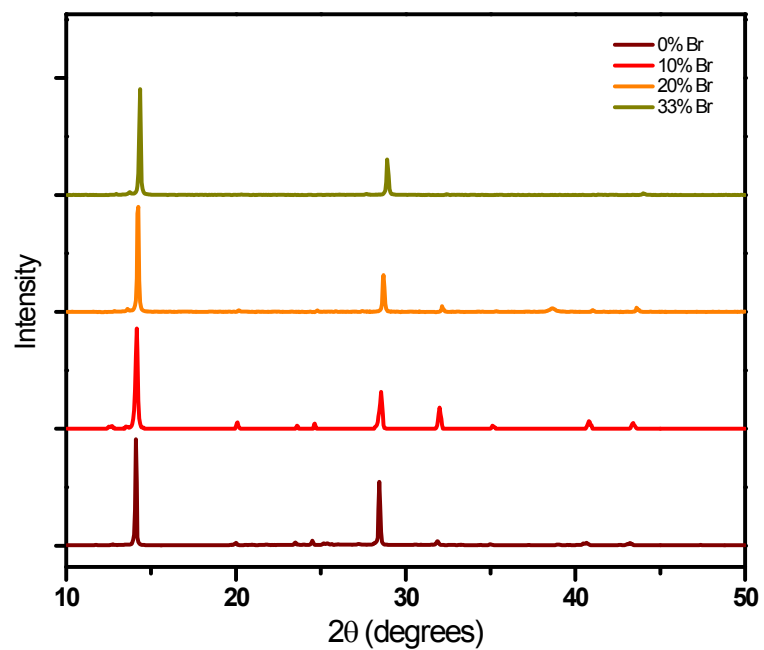**Figure S3.** Full XRD spectra of DMF-produced perovskite films.

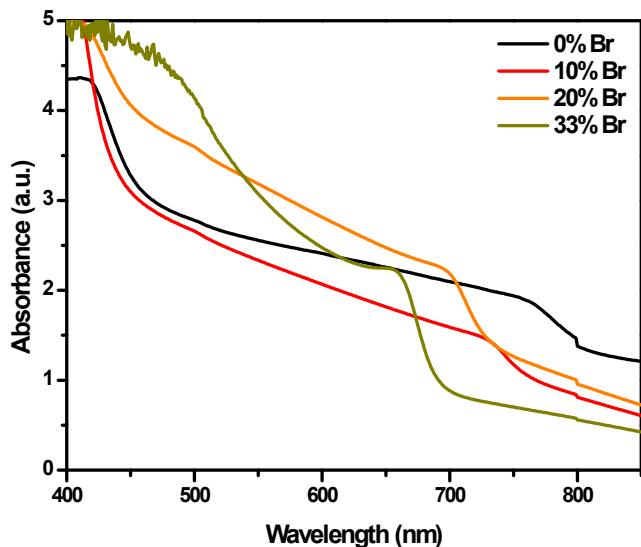**Figure S4.** Full XRD spectra of DMSO:GBL-produced perovskite films.

Figure S5. Absorbance spectra of MAPb($I_{1-x}Br_x)_3$ films deposited from 3:7 v/v DMSO:GBL show the same absorbance band edges as those from DMF, with greater variability in extinction due to film roughness.
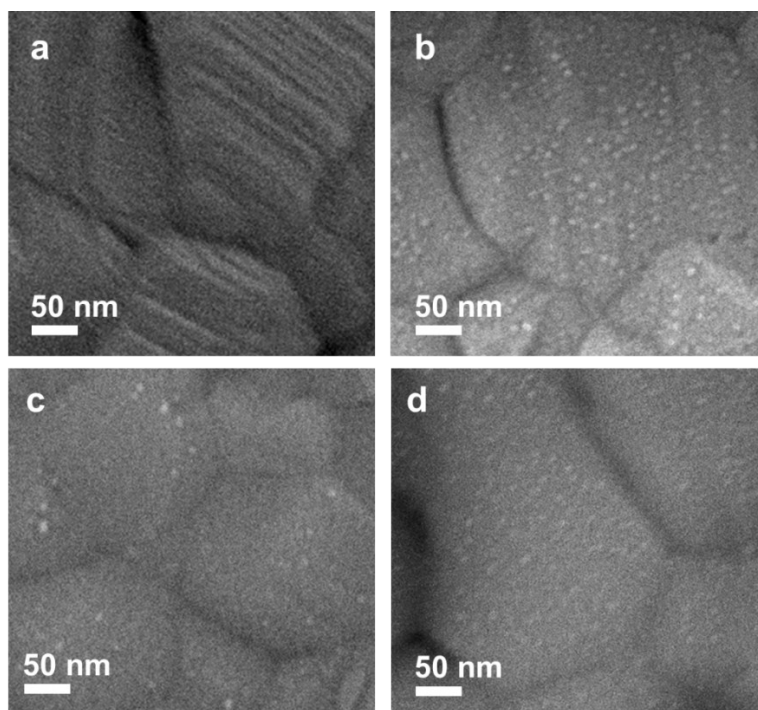

Figure S6. High-resolution SEM micrographs of (a) MAPbI$_3$, (b) MAPb($I_{0.9}Br_{0.1})_3$ (c) MAPb($I_{0.8}Br_{0.2})_3$ and (d) MAPbI$_2$Br films from DMF. Imaging over a low contrast range, we identify bright spots in Br-doped films from DMF, which we attribute to electron scattering from low-bandgap MAPbI$_3$ nuclei. We were unable to pinpoint these nuclei in any films from DMSO:GBL, however, indicating that low-bandgap recombination centers exist without a clear grain boundary within the MAPb($I_{1-x}Br_x)_3$ bulk.

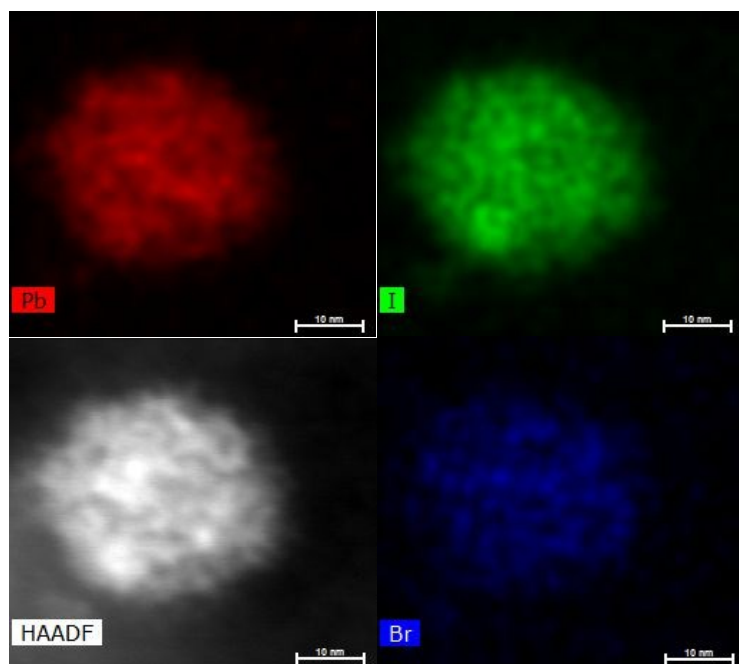**Figure S7.** STEM-EDS map of $MAPb(I_{1-x}Br_x)_3$, x=0.20 perovskite from DMF showing individual component maps. While some apparent compositional variations could stem from measurement noise, a few bright regions of Br and I counts stand out as probable pure crystals embedded within the bulk.
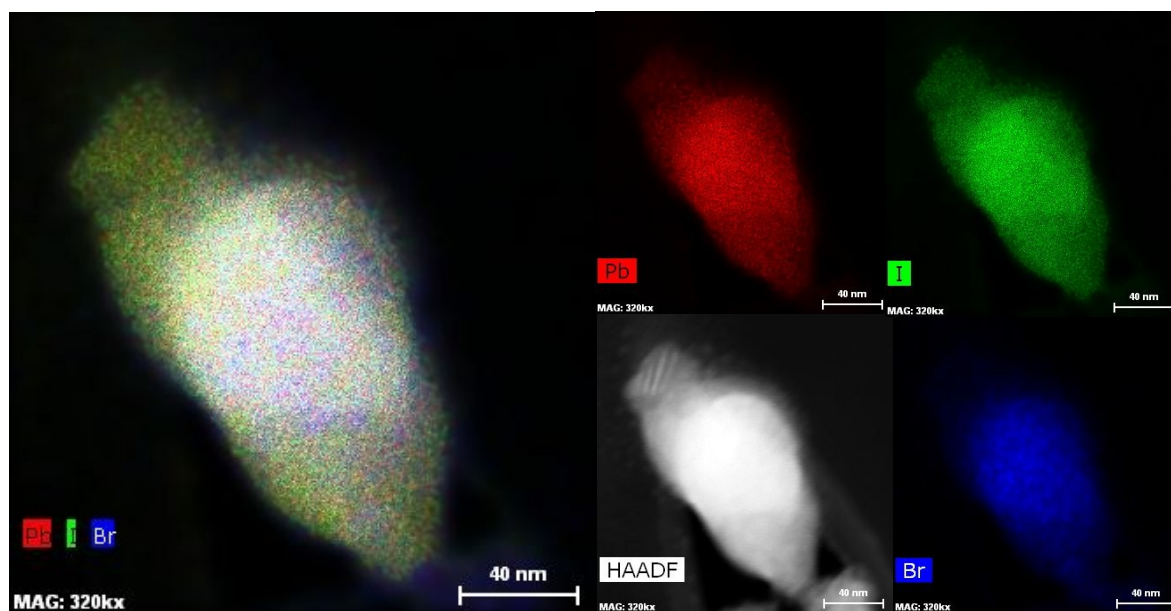

Figure S8. STEM-EDS map of $MAPb(I_{1-x}Br_x)_3$, x=0.20 perovskite from DMSO:GBL showing fewer compositional variations of I and Br. The thickness of the grain conceals any subtle compositional variations, but no discernable (~5 nm diameter or larger) $MAPbI_3$ nuclei are present in these larger perovskite grains.
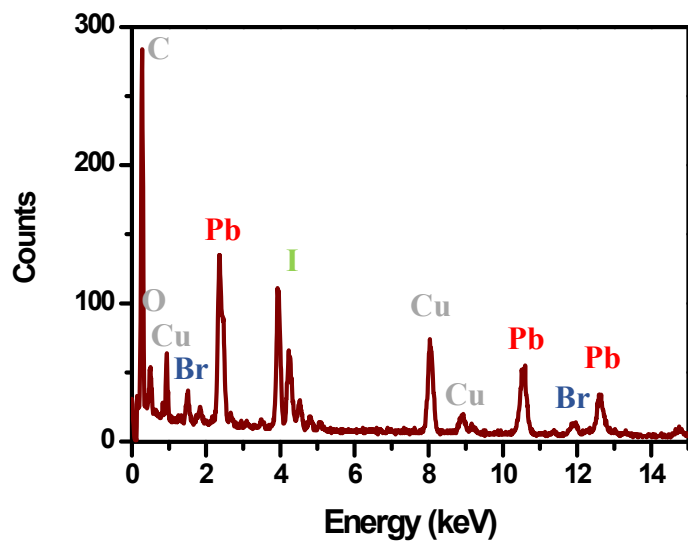
Figure S9. Energy dispersive X-ray spectrum (EDS) of $MAPb(I_{0.9}Br_{0.1})_3$ grain deposited from DMF, used for the elemental maps in Figure S6. Copper, carbon, and oxygen peaks are from the TEM grid background.